Supporting Information

Copper–Amyloid-β Targeted Fluorescent Chelator as a Potential Theranostic Agent for Alzheimer's Disease

Tao Yang,[a] Liu Yang,[a] Changli Zhang,[b] Yanqing Wang,[c] Xiang Ma,[d] Kun Wang,[d] Jian Luo,[a] Cheng Yao,*[a] Xiaoyong Wang*[e] and Xiaohui Wang*[a,d]

[a]College of Chemistry and Molecular Engineering, Nanjing Tech University, Nanjing 211816, P. R. China. E-mail: wangxhui@njtech.edu.cn

[b]Department of Chemistry, Nanjing Xiaozhuang College, Nanjing, 210017, P. R. China.

[c]Institute of Applied Chemistry and Environmental Engineering, Yancheng Teachers University, Yancheng 224002, P. R. China.

[d]State Key Laboratory of Coordination Chemistry, Nanjing University, Nanjing 210093, P. R. China.

[e]State Key Laboratory of Pharmaceutical Biotechnology, School of Life Sciences; State Key Laboratory of Analytical Chemistry for Life Science, Nanjing University, Nanjing, 210093, P. R. China.

List of Contents

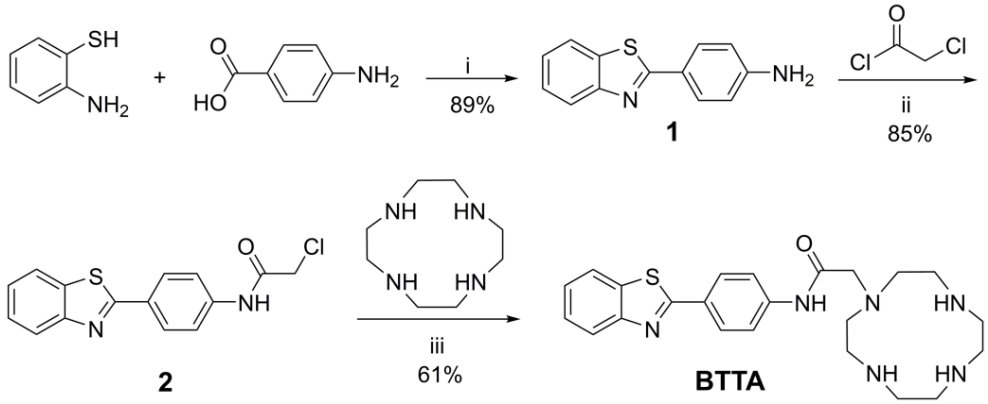

Scheme S1. Synthetic route to BTTA: (i) glycerol, 130 °C, 3 h; (ii) K_2CO_3, Acetone, 60 °C, 4 h; (iii) K_2CO_3, CH_3CN, N_2, 80 °C, overnight.

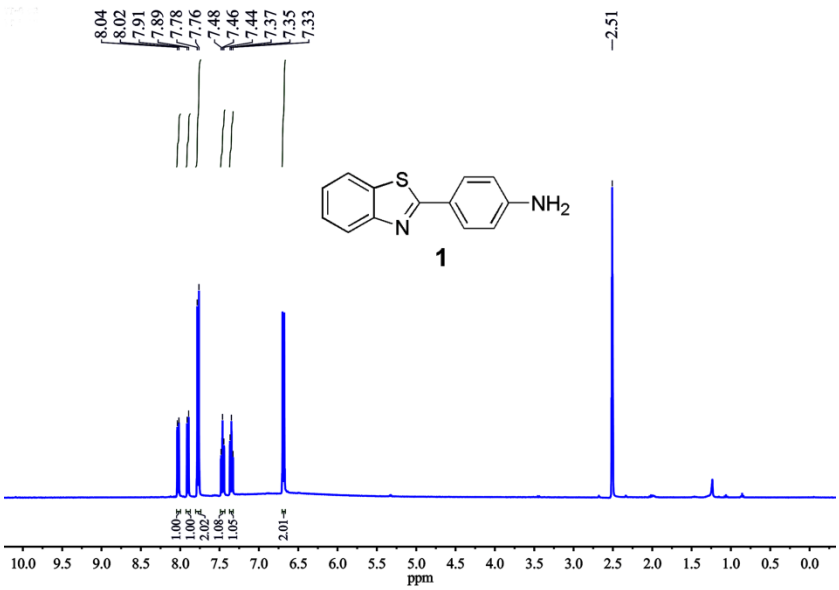

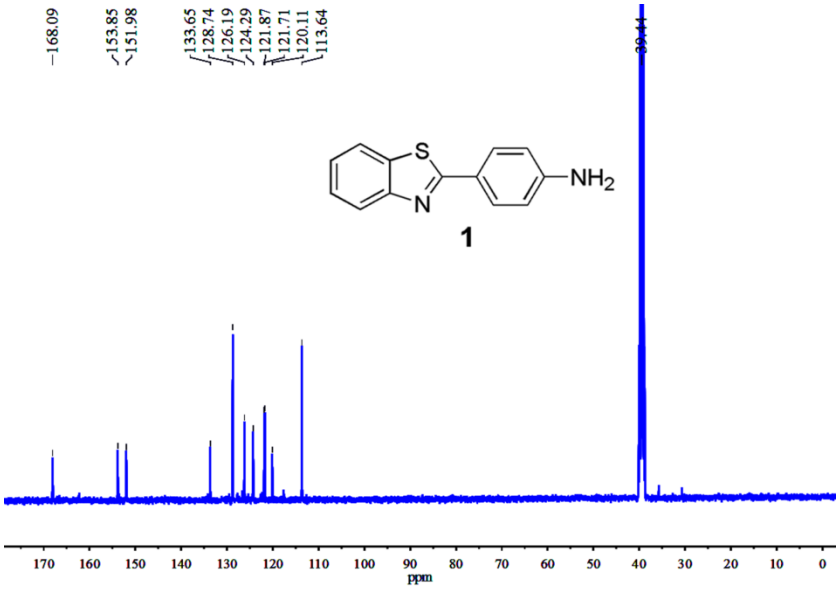

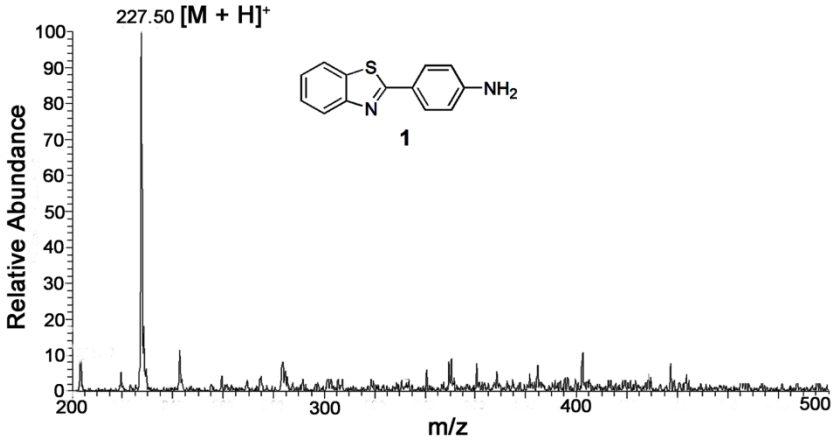

Fig. S1. ^{1}H NMR (DMSO-d_6), ^{13}C NMR (DMSO-d_6), and ESI-MS spectra for **1**.

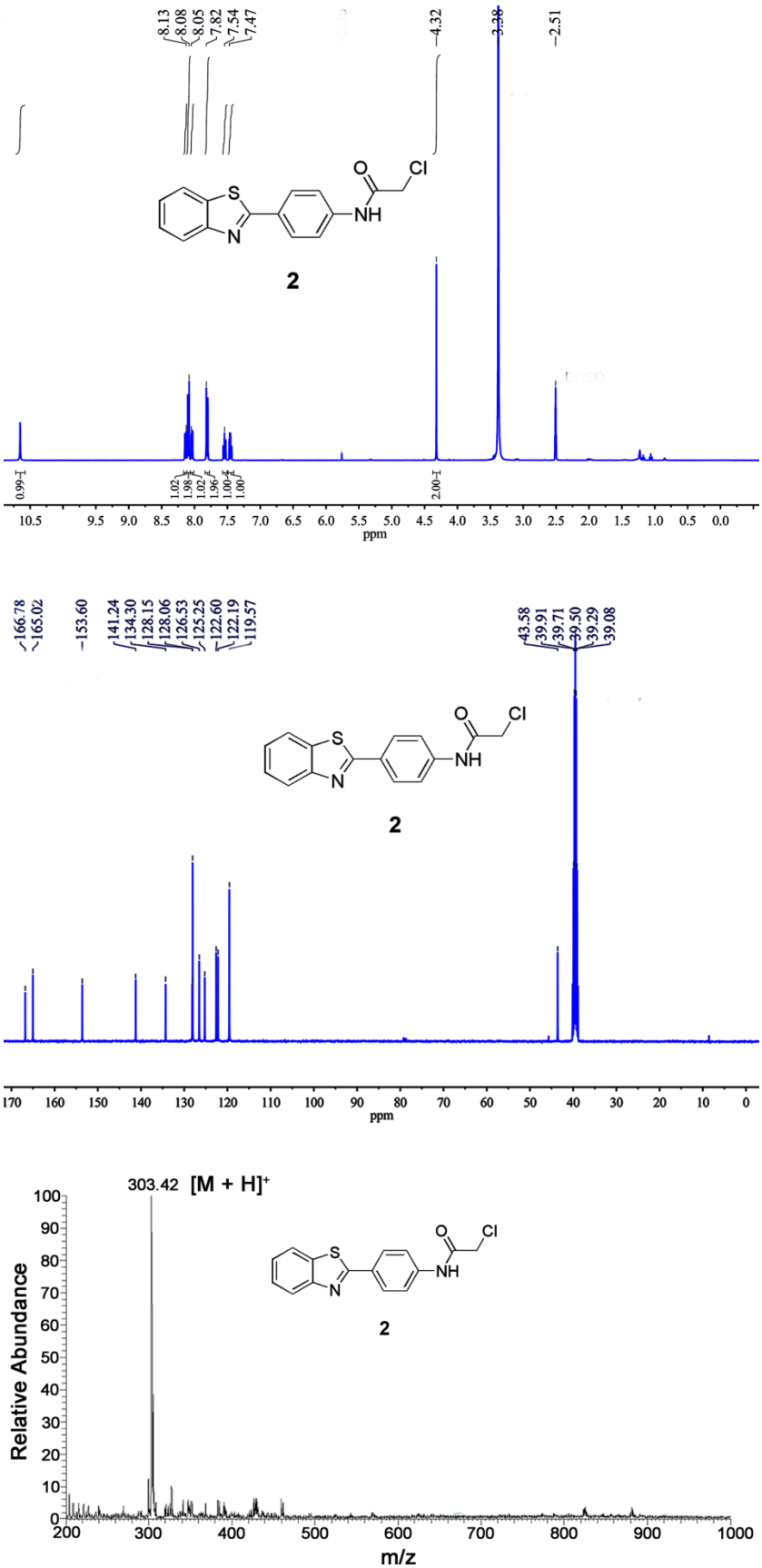

Fig. S2. ^{1}H NMR (DMSO-d_6), ^{13}C NMR (DMSO-d_6), and ESI-MS spectra for **2**.

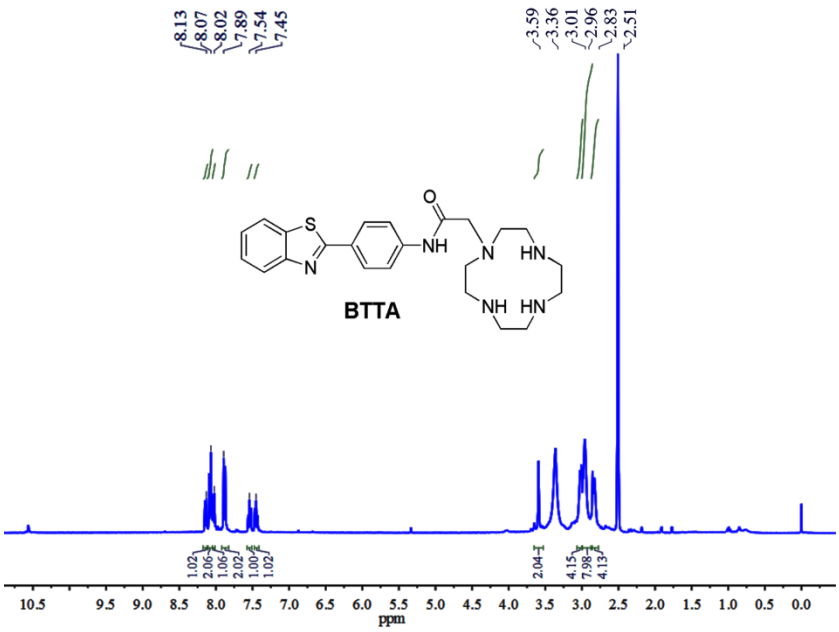

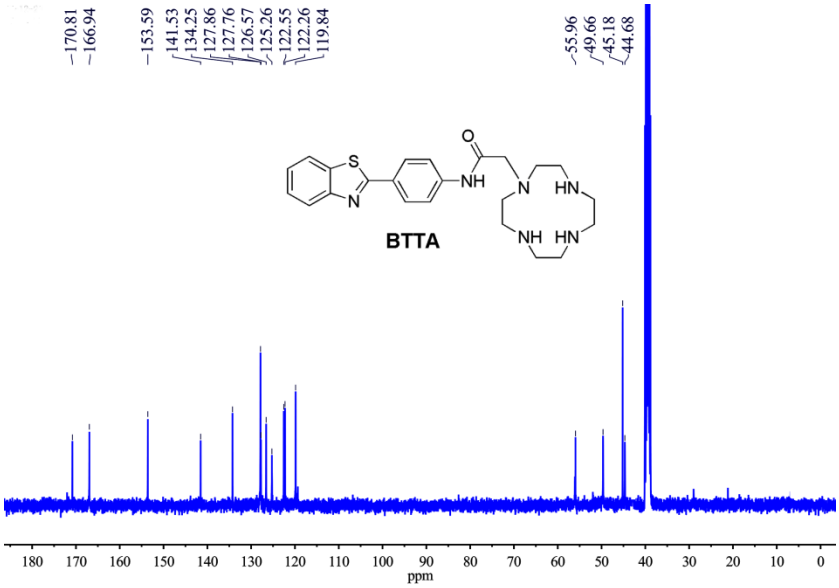

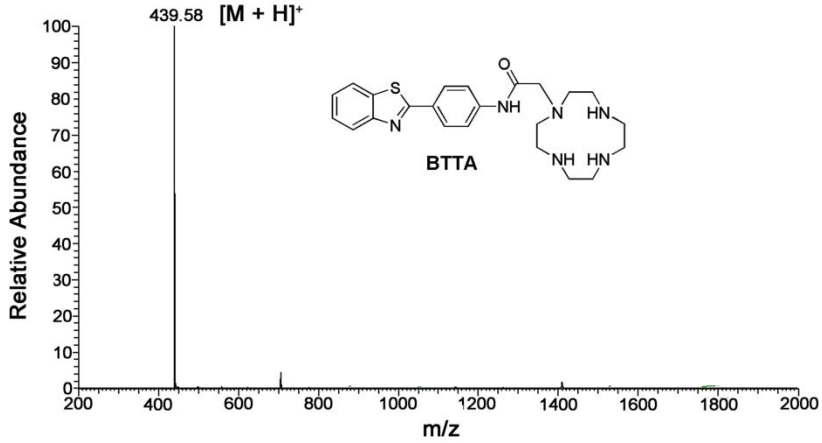

Fig. S3. ^{1}H NMR (DMSO-d_6), ^{13}C NMR (DMSO-d_6), and ESI-MS spectra for **BTTA**.

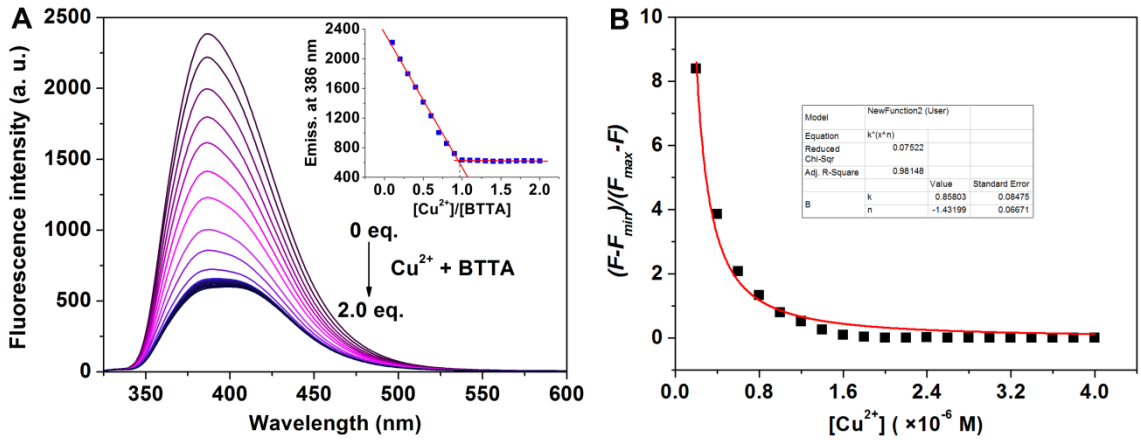

Fig. S4. (A) The fluorescence spectra of BTTA (40 μM, λ_{ex} = 318 nm) upon addition of increasing concentration of Cu^{2+} in buffer. Inset shows the emission intensity at 386 nm of BTTA versus different $[Cu^{2+}]$/[BTTA] ratio. (B) A nonlinear least-squares curve fitness with respect to the emission intensity ratio $(F-F_{min})/(F_{max}-F)$ of BTTA (2 μM, λ_{ex} = 318 nm) at 386 nm as a function of $[Cu^{2+}]$.

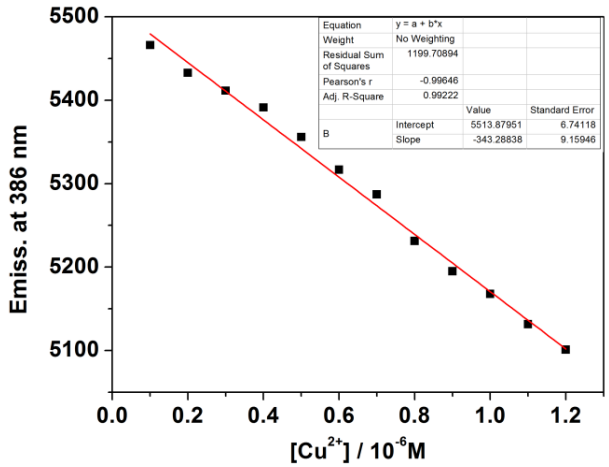

Fig. S5. Plot of fluorescence intensity of BTTA (40 μM, λ_{ex} = 318 nm) at 386 nm as a function of Cu^{2+} concentration in the range of 0 – 1.2 μM.

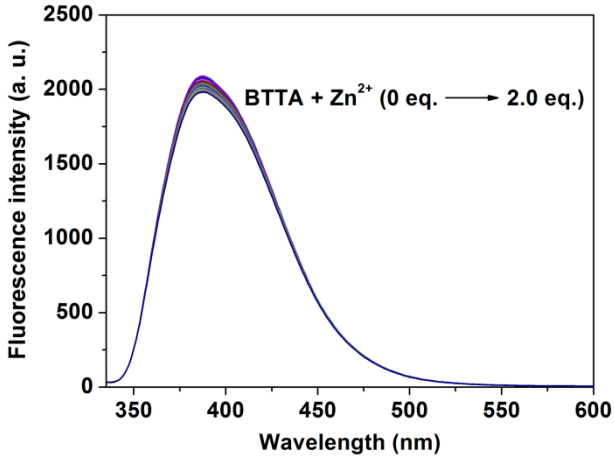

Fig. S6. The fluorescence spectra of BTTA (40 μM, λ_{ex} = 318 nm) upon addition of increasing concentration of Zn^{2+} in buffer.

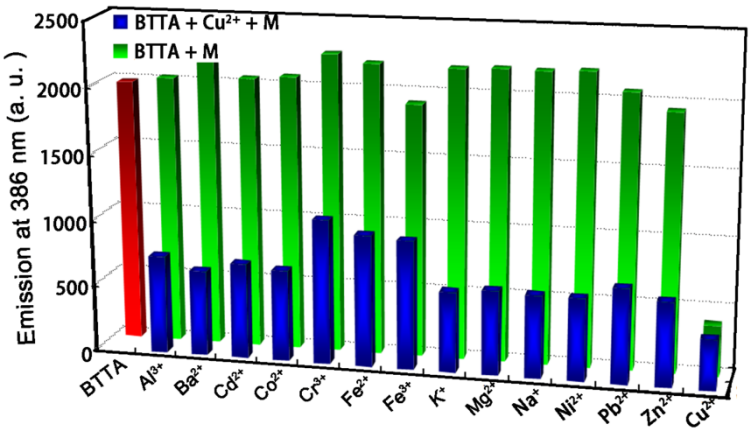

Fig. S7. Fluorescence intensity of BTTA (40 μM, λ_{ex} = 318 nm) at 386 nm in response to different metal ions (40 μM) in buffer (20 mM Tris-HCl, 150 mM NaCl, 8‰ v/v DMSO, pH 7.4). Green bars represent the addition of different metal ions to the solution of BTTA. Blue bars represent subsequent addition of Cu^{2+} to the solution.

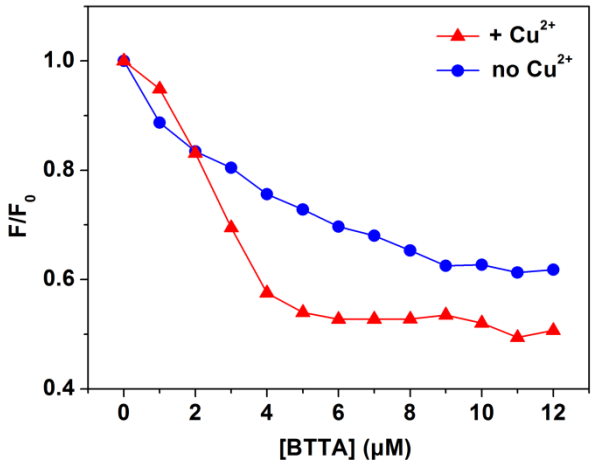

Fig. S8. The emission intensity ratio (F/F_0) of ThT (10 μM, λ_{ex} = 415 nm) at 480 nm *versus* the concentration of BTTA in the presence Aβ40 fibrils with or without Cu^{2+}.

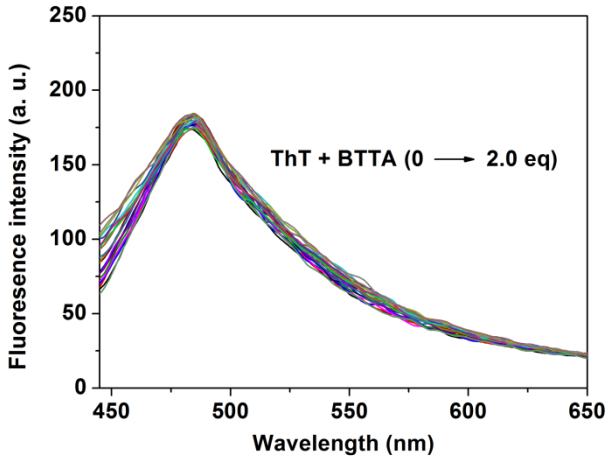

Fig. S9. The fluorescence spectra of ThT (10 μM, λ_{ex} = 415 nm) in the absence and presence of different amount of BTTA.

Table S1 Interaction energies between BTTA and responsive amino acid residues in molecular docking.

Aβ40 monomer (PDB 1BA4)[a]		Aβ40 fibrils (PDB 2LMO)[b]	
amino acid residues	interaction energy (KJ mol^{-1})	amino acid residues	interaction energy (KJ mol^{-1})
Ala2	–3.8366	Ala30(A)	–12.3098
Ala30	–2.8219	Gly33(A)	–3.7853
Asn27	–7.3316	Ile31(A)	–22.1098
Asp1	–13.6534	Ile32(A)	–23.0517
Asp23	–5.8358	Leu34(A)	–0.5448
Glu3	–13.4817	Val24(A)	–3.9239
Ile31	–19.6000	Ala21(B)	–0.9251
Leu34	–4.3672	Ala30(B)	–10.3108
Met35	–0.8664	Ile31(B)	–9.4802
Phe4	–0.4516	Ile32(B)	–15.0876
		Phe19(B)	–4.3332
		Ala21(C)	–1.2599
		Ala30(C)	–8.2647
		Gly25(C)	–8.5234
		Ile31(C)	–4.5457
		Ile32(C)	–8.2680
		Ser26(C)	–1.2037
		Val24(C)	–8.1616
		Ala21(D)	–1.2682
		Ile31(D)	–0.7862
		Ala21(E)	–0.3333
		Phe20(F)	–4.1102

[a]The MolDock score and ReRank score are –73.149 and –60.975 KJ mol^{-1}, respectively. [b]The MolDock score and ReRank score are –155.503 and –132.790 KJ mol^{-1}, respectively.

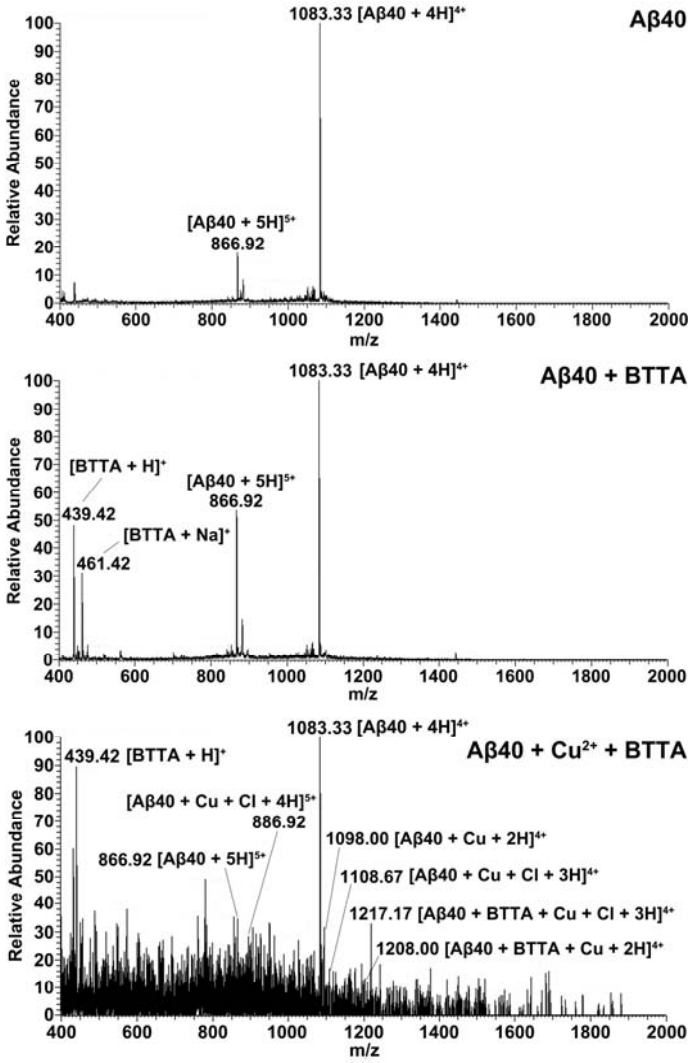

Fig. S10. ESI-MS spectra for the reaction of Aβ40 (20 μM) with or without BTTA (20 μM) in the absence or presence of Cu^{2+} (20 μM).

Table S2 Assignments of the observed peaks (m/z) in the ESI-MS spectra for the reaction of Aβ40 with or without BTTA in the absence or presence of Cu^{2+} (see Fig. S10).

Species	Formula	Obsd *m/z*	Calcd *m/z*
$[A\beta40 + 5H]^{5+}$	$C_{194}H_{300}N_{53}O_{58}S$	866.92	866.97
$[A\beta40 + 4H]^{4+}$	$C_{194}H_{299}N_{53}O_{58}S$	1083.33	1083.46
$[BTTA + H]^{+}$	$C_{23}H_{31}N_6OS$	439.42	439.60
$[BTTA + Na]^{+}$	$C_{23}H_{30}N_6NaOS$	461.42	461.58
$[A\beta40 + Cu + 2H]^{4+}$	$C_{196}H_{297}N_{53}O_{61}SCu$	1098.00	1098.87
$[A\beta40 + Cu + Cl + 4H]^{5+}$	$C_{196}H_{299}N_{53}O_{61}SClCu$	886.92	886.66
$[A\beta40 + Cu + Cl + 3H]^{4+}$	$C_{196}H_{298}N_{53}O_{61}SClCu$	1108.67	1108.67
$[A\beta40 + BTTA + Cu + 2H]^{4+}$	$C_{217}H_{324}N_{59}O_{59}S_2Cu$	1208.00	1208.55
$[A\beta40 + BTTA + Cu + Cl + 3H]^{4+}$	$C_{217}H_{325}N_{59}O_{59}S_2ClCu$	1217.17	1216.87

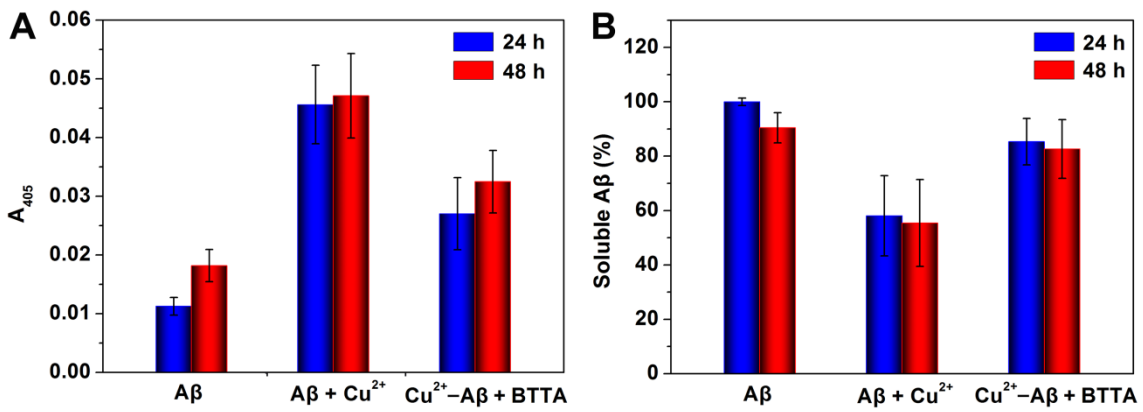

Fig. S11. The attenuation of Cu^{2+}-induced Aβ40 aggregates with different incubation time by BTTA using turbidimetry (A) and microBCA assay (B) ([Aβ40] = [BTTA] = [Cu^{2+}] = 20 μM; n = 3).

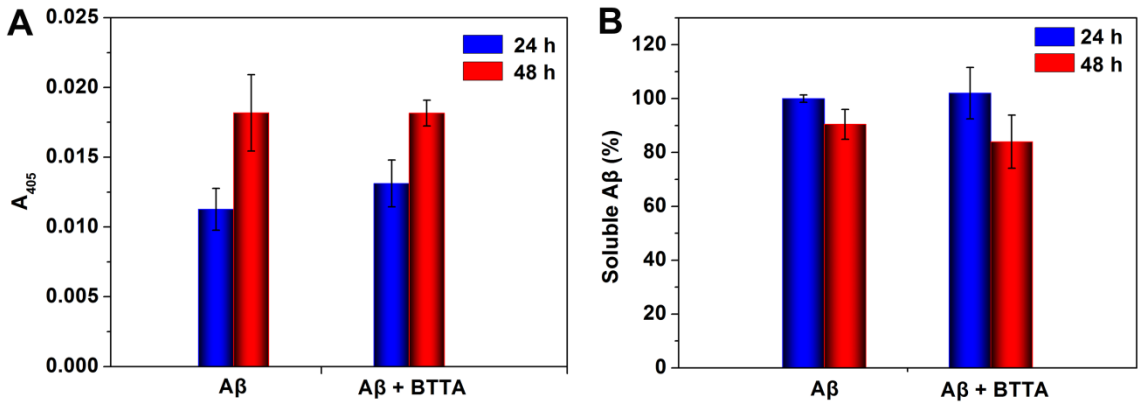

Fig. S12. The effect of BTTA on Cu^{2+}-free Aβ40 aggregates by turbidimetry (A) and microBCA assay (B) ([Aβ40] = [BTTA] = 20 μM; n = 3).

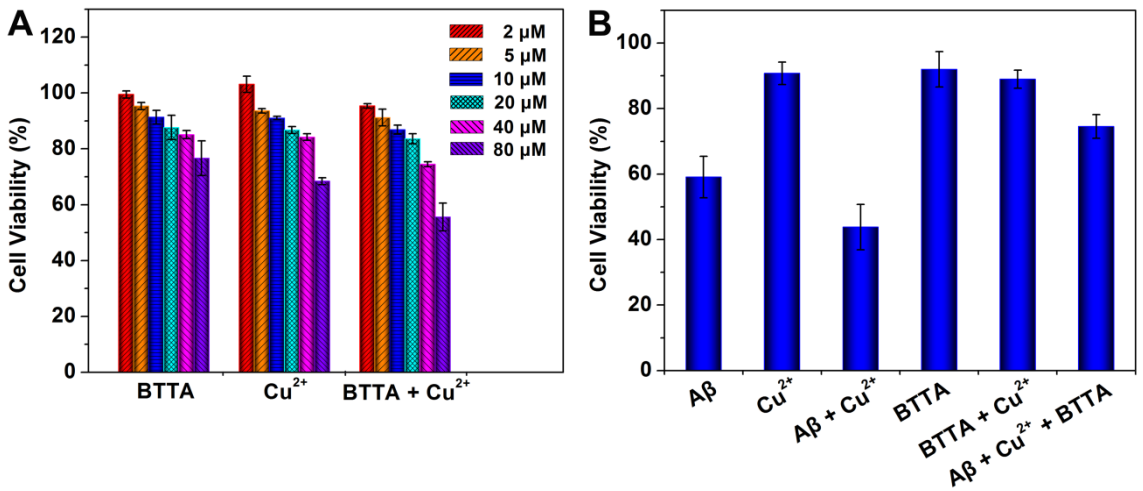

Fig. S13. Effect of BTTA on toxicity of Cu^{2+}–Aβ species in PC12 cells using an MTT assay (n = 3). (A) Cell viability (%) upon incubation of BTTA, Cu^{2+}, or BTTA + Cu^{2+} at different concentrations (2, 5, 10, 20, 40, and 80 μM, respectively) with PC12 cells for 24 h. The data were normalized and calculated as a percentage of untreated cells only containing 1% DMSO as control. (B) Attenuation of Cu^{2+}–Aβ neurotoxicity by BTTA for 24 h ([Aβ] = 10 μM; [Cu^{2+}] = 20 μM; [BTTA] = 10 μM)

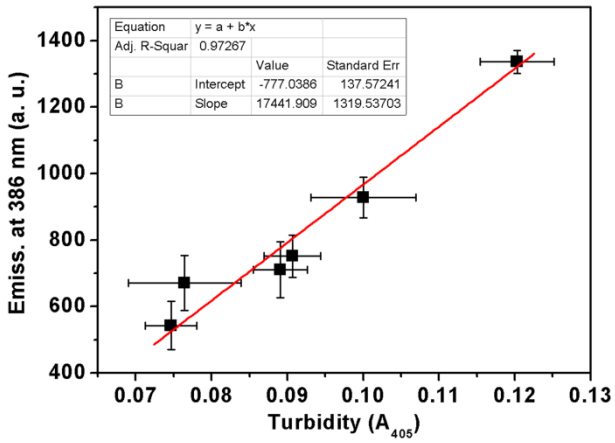

Fig. S14. The linear correlation between fluorescence intensity of BTTA (20 μM, λ_{ex} = 318 nm) at 386 nm and turbidity (A_{405}) (n =3).

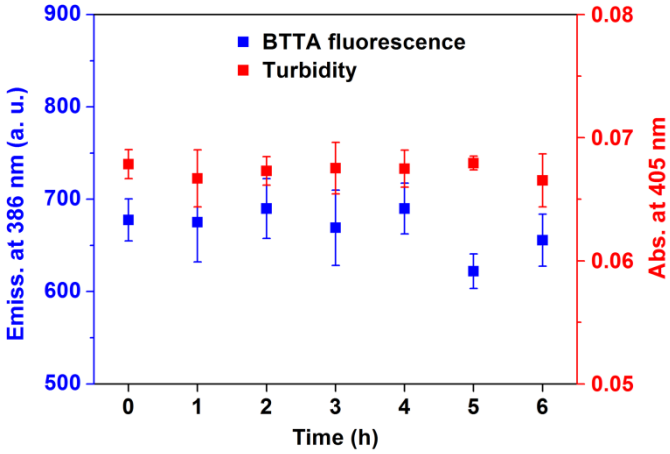

Fig. S15. Fluorescence emission intensity at 386 nm of BTTA (20 μM, λ_{ex} = 318 nm) and turbidity (A_{405}) of Cu^{2+}-free Aβ40 aggregates solution in the presence of BTTA after incubation for different periods of time (n = 3).

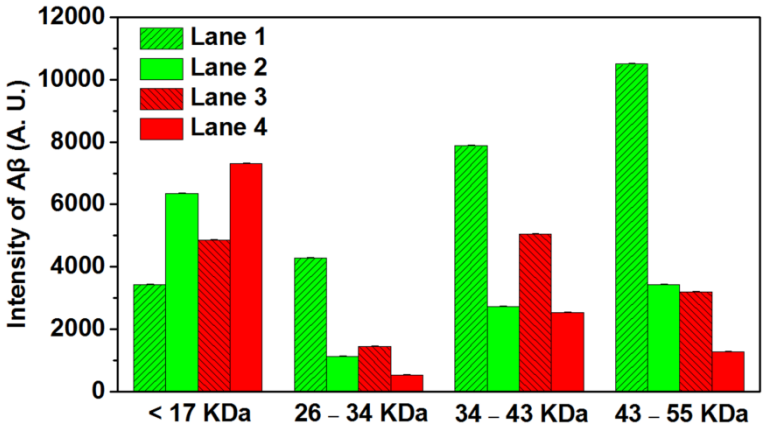

Fig. S16 Quantitative analysis of Aβ aggregates from the image of Western blot assay using the image analysis programme, ImageJ.

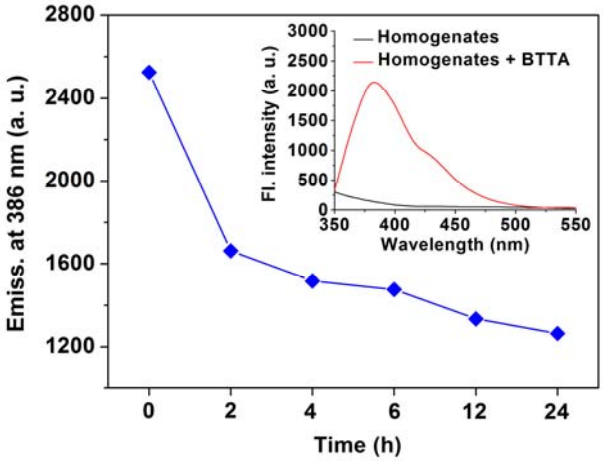

Fig. S17. Fluorescence emission intensity at 386 nm of BTTA (20 μM, λ_{ex} = 318 nm) after incubation with brain homogenates of AD mice for different periods of time. Inset shows the fluorescence spectra of brain homogenates (λ_{ex} = 318 nm) in the absence and presence of BTTA (20 μM).

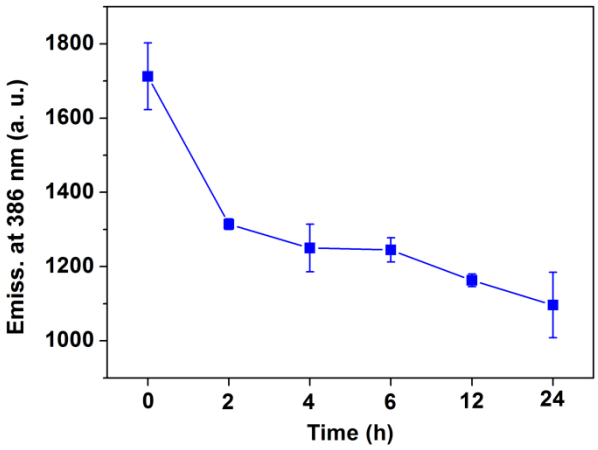

Fig. S18. Fluorescence emission intensity at 386 nm of BTTA (20 μM, λ_{ex} = 318 nm) after incubation with brain homogenates of wild-type C57BL/6J mice for different periods of time (n = 3).

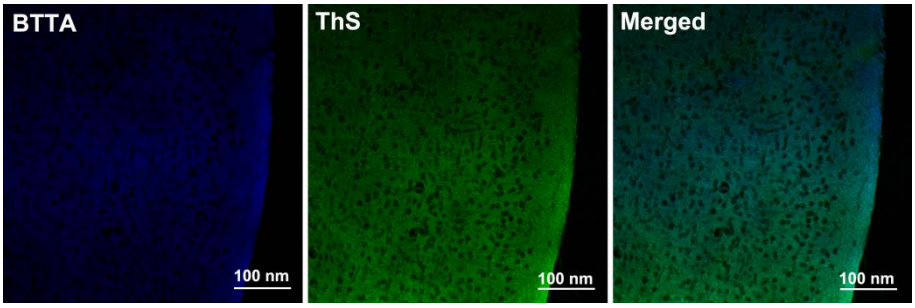

Fig. S19. Histological staining of BTTA (100 μM) on the brain slices from a wild-type C57BL/6J mouse by laser confocal microscope. The adjunct brain sections were stained with ThS.

Table S3 Molecular weight (MW), ClogP, hydrogen bond acceptors (HBA), hydrogen bond donors (HBD), polar surface area (PSA), and logBB values of BTTA.[a]

Chelators	MW	ClogP	HBA	HBD	PSA	logBB[b]
BTTA	438.59	1.618	4	4	80.79	–0.811
Lipinski's rules	≤ 450	≤ 5	≤ 10	≤ 5	≤ 90 Å^2	

[a]ClogP and PSA of BTTA were predicted by Discovery Studio 2.5 Software (Accelrys). [b]logBB = −0.0148 × PSA + 0.152 × ClogP + 0.139; compounds with logBB > 0.3 are able to cross the BBB readily, with logBB < −1.0 are only poorly distributed to the brain.

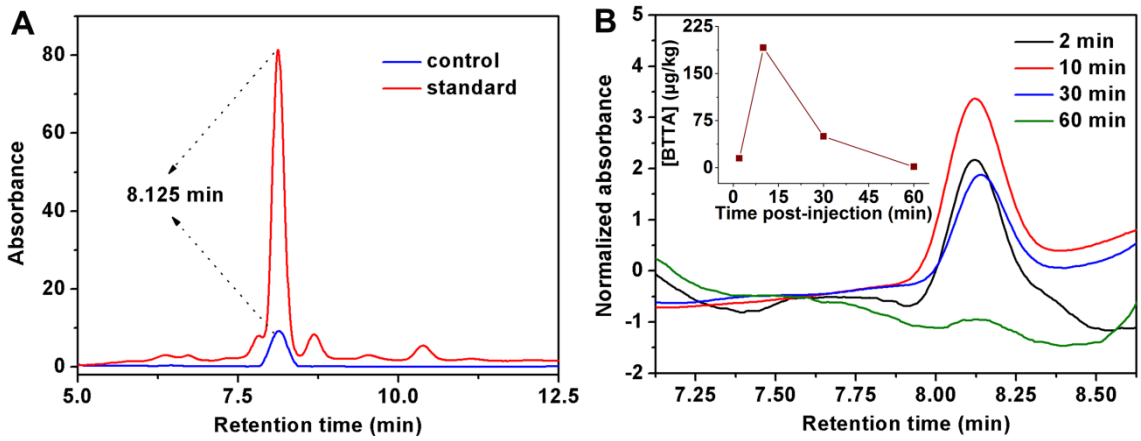

Fig. S20. (A) HPLC spectra of BTTA from control and standard samples. (B) Normalized HPLC spectra of BTTA from the brain extractions of C57BL/6J mice at different time (2, 10, 30, and 60 min) after i.v. injection. Inset: the calculated concentration of BTTA in brain tissue at different postinjection time.

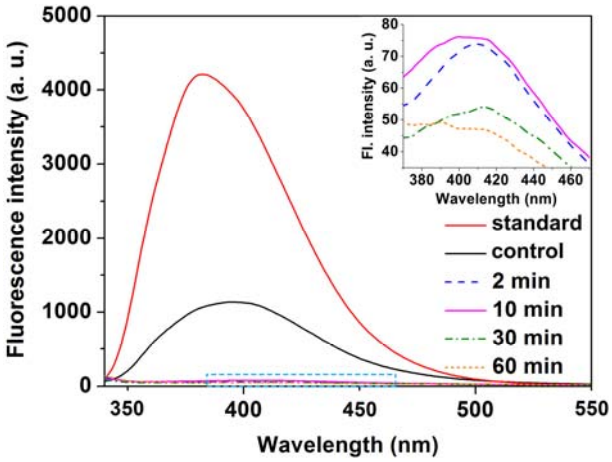

Fig. S21. Fluorescence spectra of BTTA (λ_{ex} = 318 nm) from the brain extractions of C57BL/6J mice at different postinjection time points, standard, and control samples.